

# Decomposition Products of Phosphine Under Pressure: $\text{PH}_2$ Stable and Superconducting?

Andrew Shamp, Tyson Terpstra, Tiange Bi, Zackary Falls, Patrick Avery, and Eva Zurek\*  
Department of Chemistry, State University of New York at Buffalo, Buffalo, NY 14260-3000, USA

Evolutionary algorithms (EA) coupled with Density Functional Theory (DFT) calculations have been used to predict the most stable hydrides of phosphorous ( $\text{PH}_n$ ,  $n = 1 - 6$ ) at 100, 150 and 200 GPa. At these pressures phosphine is unstable with respect to decomposition into the elemental phases, as well as  $\text{PH}_2$  and  $\text{H}_2$ . Three metallic  $\text{PH}_2$  phases were found to be dynamically stable and superconducting between 100-200 GPa. One of these contains five formula units in the primitive cell and has  $C2/m$  symmetry ( $5\text{FU-}C2/m$ ). It is comprised of 1D periodic  $\text{PH}_3\text{-PH-PH}_2\text{-PH-PH}_3$  oligomers. Two structurally related phases consisting of phosphorous atoms that are octahedrally coordinated by four phosphorous atoms in the equatorial positions and two hydrogen atoms in the axial positions ( $I4/mmm$  and  $2\text{FU-}C2/m$ ) were the most stable phases between  $\sim 160$ -200 GPa. Their superconducting critical temperatures ( $T_c$ ) were computed as being 70 and 76 K, respectively, via the Allen-Dynes modified McMillan formula and using a value of 0.1 for the Coulomb pseudopotential,  $\mu^*$ . Our results suggest that the superconductivity recently observed by Drozdov, Eremets and Troyan when phosphine was subject to pressures of 207 GPa in a diamond anvil cell may result from these, and other, decomposition products of phosphine.

PACS numbers:

## INTRODUCTION

The pressure variable can be used to synthesize materials with unique stoichiometries, and properties that would not be accessible otherwise [1–6] resulting in chemically different bonding motifs that are not observed at ambient conditions [7, 8]. Recent experimental work by Drozdov, Eremets and Troyan has shown that hydrides of the  $p$ -element sulfur are superconducting with a critical temperature,  $T_c$ , of 203 K at 150 GPa [9]. This work was inspired by first-principles calculations suggesting that at  $P > 130$  GPa  $\text{H}_2\text{S}$  would transform to a phase that has a  $T_c$  of 80 K above 160 GPa [10]. The much higher critical temperature observed experimentally led to the suggestion that under pressure hydrogen sulfide decomposes into a hydride with a stoichiometry that is not stable at 1 atm, and this new phase is responsible for the remarkably high  $T_c$  [9]. Indeed, first principles calculations [11] confirmed that the  $T_c$  (computed using the Allen-Dynes modified McMillan equation) of a novel  $Im\bar{3}m$ - $\text{H}_3\text{S}$  phase matched exceedingly well with what was observed by Drozdov and co-workers. A plethora of theoretical calculations have verified that the  $\text{H}_3\text{S}$  stoichiometry is indeed the most stable at these pressures, analyzed the factors contributing to  $T_c$ , examined anharmonicity as well as the isotope effect, and computed  $T_c$  for the related compounds selenium hydride and tellurium hydride [12–19]. These studies highlight that new hydrogen-rich materials can be attained under pressure, some of which may have a  $T_c$  higher than those previously thought possible for Bardeen-Cooper-Schrieffer (BCS)-type superconductors [20], and have invigorated the search for high-temperature superconductivity in high-pressure hydrides. For example, recently the stability of hydrides with novel stoichiometries containing a group 15 element such as P, As, and Sb have been studied computationally, and the superconducting properties of select systems were examined. [22].

Recently, new exciting experiments have revealed that

pressure-induced high-temperature superconductivity may be found in other hydrides of a  $p$ -block element. Drozdov, Eremets and Troyan measured superconductivity in phosphine,  $\text{PH}_3$ , which was liquefied in a diamond anvil cell and subsequently compressed [21]. Resistance measurements revealed a  $T_c$  of 30 K and 103 K at 83 GPa and 207 GPa, respectively. Structural information on the superconducting phases was not provided. The possible existence of a high temperature superconductor containing phosphorus and hydrogen motivated us to examine the structural landscape of these elements combined under pressure using the evolutionary algorithm XTALOPT. Similar to what was found for  $\text{H}_n\text{S}$  under pressure, it is likely that the observed superconducting properties do not arise from the hydride with the “classic” 1 atm stoichiometry, but instead decomposition products of phosphine, such as  $\text{PH}_2$ . Between the pressures of 100-200 GPa phosphine is thermodynamically less stable than  $\text{PH}_2$  and  $\text{H}_2$ , and several superconducting  $\text{PH}_2$  phases are metastable with respect to solid hydrogen and phosphorous. The  $T_c$  computed for the  $\text{PH}_2$  structures via the Allen-Dynes modified McMillan equation are significantly larger than those expected for pure phosphorus, approaching the experimental values measured in “phosphine”. Our findings therefore suggest that  $\text{PH}_2$  may be another hydrogen-rich BCS-type superconductor.

## COMPUTATIONAL DETAILS

*A priori* crystal structure prediction calculations were carried out using the open-source evolutionary algorithm (EA) XTALOPT Release 8 and 9 [23, 24] that has previously been used to predict the structures of a variety of binary hydrogen-rich phases under pressure [25–29]. EA runs were carried out on the  $\text{PH}_3$  stoichiometry at 100, 150, and 200 GPa employing simulation cells with 1-6 formula units (FU) at 100 GPa and 2-3 FU at 150 and 200 GPa. In addition, structure searches were performed on the  $\text{PH}_n$ ,  $n = (1,2,4-6)$ , systems at 100, 150, and

200 GPa using cells with 2-3 formula units, unless otherwise noted in Tables S1-S6 in the Supplementary Information (SI). Duplicate structures were detected via the XTALCOMP [30] algorithm. The lowest enthalpy structures from each search were relaxed in a pressure range from 100-200 GPa.

Geometry optimizations and electronic structure calculations were performed by using density functional theory as implemented in the Vienna *Ab-Initio* Simulation Package (VASP) versions 5.2 and 5.4.1 [31], with the gradient-corrected exchange and correlation functional of Perdew-Burke-Ernzerhof (PBE) [32]. The projector augmented wave (PAW) method [33] was used to treat the core states, and a plane-wave basis set with an energy cutoff of 700 eV was employed. The H  $1s$  and P  $3s/3p$  electrons were treated explicitly in all of the calculations, using the POTCARs for PAW-PBE H and PAW-PBE P available in the potpaw-PBE.52.tar.gz file from the VASP repository. The  $k$ -point grids were generated using the  $\Gamma$ -centered Monkhorst-Pack scheme, and the number of divisions along each reciprocal lattice vector was chosen such that the product of this number with the real lattice constant was 30 Å in the structure searches, and 40-50 Å otherwise. The  $k$ -meshes and energy cutoffs used resulted in enthalpies that were converged to within 1 meV/atom. It is likely important to employ density functionals approximating the effects of van der Waals (vdW) interactions for molecular solids containing  $p$ -block elements near ambient pressure. However, it has been shown that at higher pressures the effect of vdW interactions for these types of systems becomes negligible. For example, by  $\sim 40$  GPa dispersion forces were expected to have a minimal effect on the structural parameters, and as a result the properties, of CO<sub>2</sub> [34]. For this reason we expect the effect of vdW interactions on the results presented herein, which were obtained between 100 and 200 GPa, to be small. The Nudged Elastic Band (NEB) method [35] was used to construct a reaction pathway between the  $I4/mmm$  and  $C2/m$  PH<sub>2</sub> phases at 200 GPa.

Phonon calculations were performed using the Quantum Espresso (QE) [36] program to obtain the dynamical matrix and electron-phonon coupling (EPC) parameters. In the QE calculations, the H and P pseudopotentials, obtained from the QE pseudopotential library, were generated by the method of Trouiller-Martins with  $1s^2$  and  $3s^23p^3$  valence configurations, respectively, along with the PBE generalized gradient approximation. Plane-wave basis set cutoff energies were set to 80 Ry for all systems. The Brillouin-zone sampling scheme of Methfessel-Paxton using a smearing of 0.02 Ry and  $22 \times 22 \times 22$   $k$ -point grids were used for all 100 GPa calculations of the PH<sub>2</sub>  $2FU-C2/m$  and  $I4/mmm$  structures. At 150 and 200 GPa we used  $k$ -point grids of  $24 \times 24 \times 24$  and  $30 \times 30 \times 30$  for the PH<sub>2</sub>  $2FU-C2/m$  and  $I4/mmm$  structures, respectively. For the PH<sub>2</sub>  $5FU-C2/m$  structure a  $12 \times 12 \times 12$   $k$ -point grid was used. Density functional perturbation theory as implemented in QE was employed for the phonon calculations. The EPC matrix elements were calculated using  $2 \times 2 \times 2$   $q$ -meshes for all of the structures at 100 GPa, as well as for PH<sub>2</sub>  $5FU-C2/m$  at 150 GPa, and the phosphorus structures at

all pressures. At 150 and 200 GPa  $4 \times 4 \times 4$  and  $5 \times 5 \times 5$   $q$ -meshes were used for the PH<sub>2</sub>  $2FU-C2/m$  and  $I4/mmm$  structures, respectively. The EPC parameter,  $\lambda$ , was calculated using a set of Gaussian broadenings in steps of 0.005 Ry from 0-0.300 Ry. The broadening for which  $\lambda$  was converged to within 0.05 was between 0.015 and 0.040 Ry for all structures. The critical superconducting temperature,  $T_c$ , has been estimated using the Allen-Dynes modified McMillan equation [37] as,

$$T_c = \frac{\omega_{\log}}{1.2} \exp \left[ \frac{1.04(1 + \lambda)}{\lambda - \mu^*(1 + 0.62\lambda)} \right] \quad (1)$$

where  $\omega_{\log}$  is the logarithmic average frequency and  $\mu^*$  is the renormalized Coulomb potential, often assumed to be between 0.1 and 0.2.

## RESULTS AND DISCUSSION

### PH<sub>*n*</sub>: Pressure Induced Decomposition of PH<sub>3</sub>

Because the phases that PH<sub>3</sub> adopts under pressure are unknown, we have carried out evolutionary searches to predict the global minima configurations up to 200 GPa. A detailed analysis will be published elsewhere, but the coordinates for the most stable structures found at  $P \geq 100$  GPa are provided in the SI. Briefly, the 100 GPa phase is made up of layers of PH and hydrogen, whereas the 150 and 200 GPa structures consist of 1-dimensional (1D) PH<sub>3</sub>-PH<sub>3</sub> networks that resemble those present in the most stable PH<sub>2</sub> structure at 100 GPa discussed below. The computed enthalpies of formation,  $\Delta H_f$ , of PH<sub>3</sub> with respect to the most stable structures of solid hydrogen [38, 39] and phosphorus [40–44] showed that the classic 1 atm stoichiometry is not thermodynamically stable at the pressures considered herein, and potentially even at lower pressures. The  $\Delta H_f$  for the reaction  $\frac{3}{2}\text{H}_2(\text{s}) + \text{P}(\text{s}) \rightarrow \text{PH}_3$  were computed to be 58.0, 45.2, and 42.6 meV/atom at 100, 150, and 200 GPa, respectively.

Nonetheless, it is convenient to plot the  $\Delta H_{\text{rxn}}$  of the hydrides of phosphorous, PH<sub>*n*</sub> with  $n = 1 - 6$ , identified via our evolutionary searches for the reaction  $\text{PH}_n \rightarrow (\frac{3-n}{3})\text{P} + (\frac{n}{3})\text{PH}_3$  (where  $n = 0 - 3$ ) and  $\text{PH}_n \rightarrow (\frac{n-3}{2})\text{H}_2 + \text{PH}_3$  (where  $n = 3 - 6$ ), as shown in the left and right hand sides of Fig. 1(a), respectively. For each of these plots a convex hull can be drawn, and the structures whose  $\Delta H_{\text{rxn}}$  lie on the hull correspond to the most stable decomposition products of phosphine, or the most stable products arising from the reaction of phosphine with hydrogen. At 100, 150 and 200 GPa only PH<sub>2</sub> is thermodynamically preferred over P/PH<sub>3</sub>, and the reaction  $\text{PH}_3 \rightarrow \text{PH}_2 + \frac{1}{2}\text{H}_2$  is exothermic. At 100 and 150 GPa the reaction  $\text{PH}_3 + \text{H}_2 \rightarrow \text{PH}_5$  is exothermic. Because PH<sub>5</sub> becomes unstable by 200 GPa we focused our analysis on PH<sub>2</sub> (the coordinates for PH<sub>5</sub> are provided in the SI).

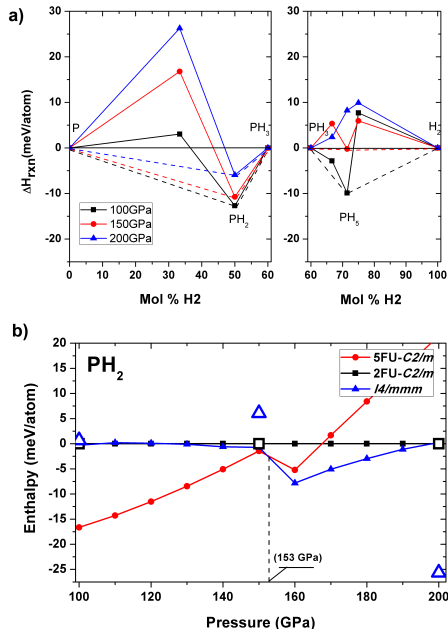


FIG. 1: (a)  $\Delta H_{\text{rxn}}$  for the reaction: (left)  $\text{PH}_n \rightarrow (\frac{3-n}{3})\text{P} + (\frac{n}{3})\text{PH}_3$  (where  $n = 0 - 3$ ) and (right)  $\text{PH}_n \rightarrow (\frac{n-3}{2})\text{H}_2 + \text{PH}_3$  (where  $n = 3 - 6$ ) at 100, 150, and 200 GPa. The convex hulls are given by the dashed lines. (b) The enthalpies as a function of pressure for the 5FU- $C2/m$  and  $I4/mmm$  phases of  $\text{PH}_2$  relative to 2FU- $C2/m$  between 100-200 GPa. The dashed line indicates the transition pressure below which the 5FU- $C2/m$  phase has the lowest non-ZPE corrected enthalpy. The open symbols provide the relative enthalpies including the ZPE correction. At 150 GPa the ZPE-corrected enthalpy of 5FU- $C2/m$  (not shown on the plot) is 45.8 meV/atom higher than that of the 2FU- $C2/m$  structure.

Evolutionary searches at 100, 150 and 200 GPa identified three unique low-enthalpy  $\text{PH}_2$  phases, whose relative enthalpies are provided in Fig. 1(b). A  $C2/m$  symmetry system whose primitive cell contained five formula units, 5FU- $C2/m$ , had the lowest enthalpy excluding zero point energy (ZPE) contributions below 153 GPa. A two formula unit cell with  $C2/m$  symmetry (2FU- $C2/m$ ) and an  $I4/mmm$  structure became preferred at higher pressures. Even though these species are thermodynamically unstable relative to solid phosphorous and  $\text{H}_2$  (by at least 38.7, 29.4, and 31.9 meV/atom at 100, 150 and 200 GPa), they are all dynamically stable at 100, 150 and 200 GPa. Moreover, the formation of  $\text{PH}_n$  with  $n = 4 - 6$  from  $\text{PH}_2$  and  $\text{H}_2$  at 100, 150 and 200 GPa, and the decomposition of  $\text{PH}_2$  into  $\text{H}_2$  and  $\text{PH}$  at 100 and 150 GPa is computed as being endothermic.

The coordination and arrangement of the phosphorus atoms in 5FU- $C2/m$  is quite different than in the 2FU- $C2/m$  and  $I4/mmm$  phases. The former consists of  $\text{PH}_3$ - $\text{PH}$ - $\text{PH}_2$ - $\text{PH}$ - $\text{PH}_3$  oligomers extending along the  $c$ -axis, which are 1D periodic along the  $a$ -axis,  ${}^1_\infty[\text{PH}_3\text{-PH-PH}_2\text{-PH-PH}_3]$ , see Fig. 2(a,b). The  $\text{PH}_3\text{-PH-PH}_2\text{-PH-PH}_3$  unit possesses an inversion

center of symmetry, with the  $\text{H}_3\text{P-PH}$  and  $\text{HP-PH}_2$  distances measuring 2.191 and 2.167 Å, respectively, at 100 GPa. The phosphorous atoms comprising the  $\text{PH}$  and  $\text{PH}_2$  units are coordinated to four other phosphorous atoms forming a square net. Such structural motifs are not uncommon for compressed phosphorous, particularly in the pressure range between 100-200 GPa. For example, a number of the high pressure phases of elemental phosphorus, such as the A17 and A7 phases, have been described as Peierls distortions of a simple cubic lattice [41, 45, 46]. Beyond the A7 phase of black phosphorus, a simple cubic lattice is adopted at  $\sim 11.1$  GPa that is stable up to 137 GPa [40, 42, 44]. After a relatively brief transition through a suspected incommensurate phase [47, 48], simple cubic phosphorus transitions into a simple hexagonal phase [42] followed by a body centered cubic phase adopted at pressures above 262 GPa [43].

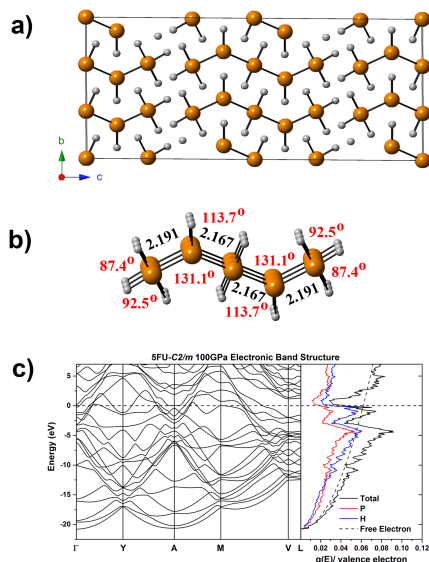


FIG. 2: (a) A  $3 \times 3 \times 2$  supercell of the 100 GPa 5FU- $C2/m$  structure. Phosphorous atoms are orange, hydrogen atoms are white. (b) A fragment of the  ${}^1_\infty[\text{PH}_3\text{-PH-PH}_2\text{-PH-PH}_3]$  motifs that comprise 5FU- $C2/m$ . The values provided in black are P-P distances (Å) and the red values are bond angles at 100 GPa. (c) Electronic band structure along with the total and site projected electronic DOS of 5FU- $C2/m$  at 100 GPa. Because the PDOS for the H and P atoms were relatively independent upon the local atomic environment, we have not decomposed the PDOS into contributions from distinct H and P atoms.  $E_F$  is set to zero.

The phosphorous atoms in the  $-\text{PH}_3$  units at the end of the oligomer are nearly perfectly octahedrally coordinated to three hydrogen and three phosphorous atoms, with the H-P-H angles measuring 87.4 and 92.5° and the P-P-P angles measuring 90° at 100 GPa. Similarly, the phosphorous atoms comprising the  $-\text{PH}_2-$  units at the center of the motif also assume octahedral coordination with four phosphorous atoms on the equatorial and two hydrogen atoms on the axial positions. The phosphorous atoms within the  $-\text{PH}-$  segment of the oligomer,

on the other hand, are nearly trigonal bipyramidal. The axial positions are occupied by two phosphorous atoms, and the equatorial positions are filled by two phosphorous and one hydrogen atom ( $\angle PPP = 131.1^\circ$ ,  $\angle PPH = 113.7$  and  $115.2^\circ$ ). At this pressure all of the P-H distances fall between 1.430-1.444 Å, which is close to the typical experimental P-H bond length of 1.437 Å [49] at 1 atm. The P-P distances fall in the range of 2.167-2.191 Å within the oligomer, and measure 2.151 Å between oligomers, which is comparable to the distance we calculate for elemental phosphorous at this pressure, 2.149 Å.

Fig. 2(c) shows that at 100 GPa 5FU- $C2/m$ -PH<sub>2</sub> is metallic. The occupied density of states (DOS) is nearly free electron like. But because the Fermi level,  $E_F$ , falls near a pseudogap the DOS at  $E_F$ ,  $g(E_F) = 0.045 \text{ eV}^{-1}/\text{valence electron}$ , is lower than the value computed for a free electron gas with the same bandwidth,  $0.063 \text{ eV}^{-1}/\text{valence electron}$ . The metallicity is due primarily to hydrogen states with  $s$ -character and also phosphorous states with  $p$ -character. The occupied hydrogen and phosphorous states hybridize, indicative of covalent bonding. The electron localization function (ELF), provided in the SI, shows regions of high ELF along the P-P and P-H bonds, and no lone pairs are observed, as would be expected based upon valence-shell electron-pair repulsion (VSEPR) theory, which assumes that the geometry a molecule assumes minimizes the repulsion between valence shell electron pairs. A Bader analysis revealed electron transfer from phosphorous to hydrogen, with the average charge on the hydrogen atoms being -0.34 at 100 GPa. The charges on the phosphorous atoms in the -PH<sub>3</sub>, -PH<sub>2</sub>-, and -PH- units were computed as being +1.12, +0.70 and +0.25, respectively. At 150 GPa the average Bader charges become -0.37 (H), +1.15 (P in -PH<sub>3</sub>), +0.75 (P in -PH<sub>2</sub>-) and +0.30 (P in -PH-). Phonon calculations showed that this phase is dynamically stable at 150 GPa.

Above  $\sim 160$  GPa two structurally related PH<sub>2</sub> phases, 2FU- $C2/m$  (Fig. 3) and  $I4/mmm$  (Fig. 4), become more stable than 5FU- $C2/m$ . The differences in the enthalpies of these two compounds at 150 and 200 GPa are less than 1 meV/atom, but in between these pressures the non-ZPE corrected enthalpy of the  $I4/mmm$  phase is slightly lower than that of 2FU- $C2/m$ . The existence of nearly isoenthalpic hydrogen-rich phases under pressure in the DFT calculations is not unprecedented. We have previously found nearly isoenthalpic but distinct structures in our theoretical studies of hydrides containing an alkali metal or alkaline earth metal under pressure. This includes two Li<sub>5</sub>H phases that were computed as being more stable than Li and LiH above 50 GPa [27], five unique CsH<sub>3</sub> structures that were preferred over CsH and H<sub>2</sub> between 30-150 GPa [28] and three BaH<sub>6</sub> phases that had nearly the same enthalpies around 100 GPa [51].

In both the  $C2/m$  and  $I4/mmm$  phases of PH<sub>2</sub> each phosphorous is octahedrally coordinated by four phosphorous atoms in the equatorial positions, and two hydrogen atoms in the axial positions. The difference between the two structures is that whereas in  $I4/mmm$  all of the atoms assume

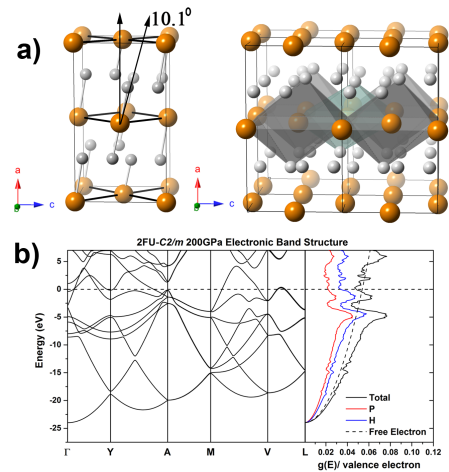


FIG. 3: (a) (left) A conventional unit cell and (right) a  $1 \times 2 \times 2$  supercell of the 200 GPa 2FU- $C2/m$  phase. Phosphorous atoms are orange, hydrogen atoms are white. (left) The canting angle with respect to a line perpendicular to the plane containing the phosphorous atoms ( $10.1^\circ$ ) is shown by the arrows. (right) The octahedra around the central plane of phosphorous atoms are highlighted by teal and gray. (b) Electronic band structure along with the total and site projected electronic DOS of 2FU- $C2/m$  at 200 GPa.  $E_F$  is set to zero.

the ideal octahedral angles, in 2FU- $C2/m$  the hydrogens are canted with respect to a line that lies normal to the phosphorous square net. At 100 GPa the canting angle is negligible ( $< 0.1^\circ$ ), and the P-P and P-H bond lengths in the two structures are nearly identical (Table I). At 160 and 200 GPa, however, the canting angle increases to 9.8 and  $10.1^\circ$ , respectively. Even though the nearest neighbor P-P/P-H distances in  $I4/mmm$  are slightly smaller than in 2FU- $C2/m$  at 160 and 200 GPa, the volume of the former is somewhat larger than that of the latter due to the tilting of the octahedra. The more efficient packing of the octahedra between the layers, which is a consequence of the canting, can most easily be seen by comparing the P-P distances between the phosphorous atoms comprising different layers. At 100 GPa the separation is identical, 2.983 Å, resulting in comparable volumes. By 160 GPa, however, this distance becomes 2.757 and 2.695 Å for  $I4/mmm$  and 2FU- $C2/m$ , respectively, giving rise to the sudden difference in volume of 1.2% between the two phases. The  $PV$  contribution to the enthalpy is smaller in the more compact 2FU- $C2/m$  phase, but the electronic contribution more strongly favors the more symmetric  $I4/mmm$  structure (see the SI), such that  $I4/mmm$  is preferred by a few meV/atom for  $P \sim 155$ -195 GPa. By 200 GPa, however, the two phases become isoenthalpic.

Similar to 5FU- $C2/m$ , regions of high ELF in 2FU- $C2/m$  and  $I4/mmm$  are found only along the P-P and P-H bonds and the Bader charges in Table I are indicative of charge transfer from phosphorous to hydrogen. Both of these phases are good metals with  $g(E_F) = 0.045$ - $0.048 \text{ eV}^{-1}/\text{valence electron}$

TABLE I: Phosphorus-phosphorus, phosphorus-hydrogen and hydrogen-hydrogen distances for the  $2\text{FU-}C2/m$  and  $I4/mmm$   $\text{PH}_2$  phases. P-H(1)/H-H(1) are the first nearest neighbor, and P-H(2) are the second nearest neighbor distances. The average Bader charges per atom type are provided, along with the volume per unit cell.

System	Pressure (GPa)	P-H(1) ( $\text{\AA}$ )	P-H(2) ( $\text{\AA}$ )	P-P ( $\text{\AA}$ )	H-H(1) ( $\text{\AA}$ )	H ( $e$ )	P ( $e$ )	Volume ( $\text{\AA}^3/\text{FU}$ )
$2\text{FU-}C2/m$	100	1.449	2.165	2.159	1.527	-0.26	0.53	13.885
	150	1.436	2.013	2.111	1.497	-0.29	0.57	12.398
	160	1.445	1.760	2.127	1.510	-0.27	0.55	12.025
$I4/mmm$	200	1.439	1.693	2.093	1.500	-0.26	0.52	11.288
	100	1.449	2.163	2.157	1.528	-0.30	0.60	13.882
	150	1.437	2.012	2.109	1.494	-0.28	0.56	12.401
	160	1.435	1.989	2.101	1.490	-0.28	0.56	12.170
	200	1.434	1.896	2.077	1.487	-0.26	0.52	11.359

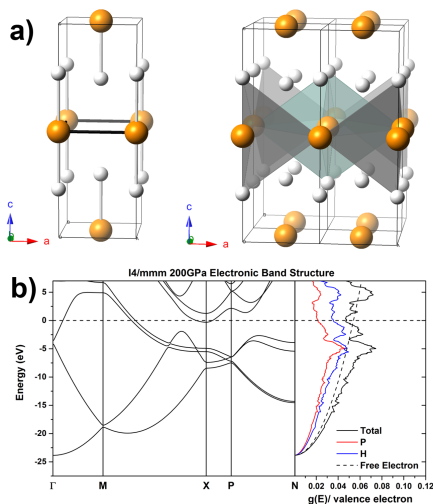


FIG. 4: Same as Fig. 3 except for  $I4/mmm$   $\text{PH}_2$  at 200 GPa.  $\angle\text{PPP}=90^\circ$ ,  $\angle\text{HPP}=90^\circ$  and  $\angle\text{HPH}=180^\circ$ . In the figure on the top right a  $2\times 2\times 1$  supercell is shown.

at 200 GPa, which is close to the value computed for a free electron gas with the same bandwidth,  $0.054 \text{ eV}^{-1}/\text{valence electron}$ . Their DOS plots display many features in common with the DOS calculated for  $5\text{FU-}C2/m$ : they are indicative of H/P hybridization and the character at the Fermi level is primarily hydrogen  $s$ -like, with substantial contributions from phosphorous  $p$ -states. Phonon calculations revealed that these two structures are dynamically stable at 100, 150, and 200 GPa.

Because of the structural similarity between the  $2\text{FU-}C2/m$  and  $I4/mmm$  phases, we wondered if they may be connected via a low energy pathway. The NEB method was employed to find the barrier and transition state between the two structures. The computed barrier was  $\sim 270 \text{ meV/atom}$  at 200 GPa, implying that these phases likely lie within two distinct wells on the potential energy surface. The transition state (whose coordinates are given in the SI) can best be de-

scribed as the average of the two  $\text{PH}_2$  phases. Within the NEB method, the positions of the individual atoms within the starting and ending structures must match as closely as possible to avoid large geometric changes that may result in unrealistic barriers. In order to do this the  $I4/mmm$  structure has to be reduced down to its primitive triclinic cell and then a 2 FU supercell in the crystallographic  $b$ -direction direction must be constructed. In the transition state structure the perfect  $90^\circ$  square phosphorus nets described above have been distorted to diamonds with internal angles of  $67$  and  $113^\circ$  resulting in nearest and second nearest neighbor P-P distances of  $1.885$  and  $2.581 \text{ \AA}$  (c.f. Table 1), and the distance separating the P-P layers is  $2.941 \text{ \AA}$ , which can be compared to  $3.017$  and  $2.963 \text{ \AA}$  for the  $I4/mmm$  and  $C2/m$  phases, respectively. Each phosphorus is  $[2+4]$  coordinate to hydrogen. Similar to the two end point structures, the shortest two P-H distances fall between  $1.45$  and  $1.50 \text{ \AA}$ , which is slightly longer than the distance of a P-H bond in phosphine at ambient conditions,  $1.42 \text{ \AA}$  [50]. The remaining four P-H distances fall within  $1.7$ - $1.8 \text{ \AA}$ , and are different for each phosphorous atom in the  $P1$  symmetry  $2\text{FU}$  transition state.

We also wondered if tilting the octahedra to different angles would yield other structures not found in our evolutionary runs whose enthalpies were similar to  $I4/mmm$  and  $C2/m$ . In order to test this hypothesis we relaxed structures constructed to have canting angles of  $45^\circ$ , as well as geometries where hydrogen atoms were placed at random positions within the phosphorous lattice at 200 GPa. No unique low enthalpy structures were found. In addition, a closer inspection of the evolutionary runs showed that structures similar to those we constructed by hand had been generated and optimized during the EA searches, but their enthalpies were significantly higher than  $5\text{FU-}C2/m$ ,  $2\text{FU-}C2/m$  and  $I4/mmm$   $\text{PH}_2$ .

Because the ZPE may be large for extended systems containing light elements, we computed the enthalpic differences between these three  $\text{PH}_2$  phases including the ZPE corrections at pressures where they were dynamically stable. The open symbols in Fig. 1(c) show that the inclusion of the ZPE makes the  $I4/mmm$  and  $2\text{FU-}C2/m$  structures significantly more stable than  $5\text{FU-}C2/m$  at 150 GPa, with the  $C2/m$  be-



ing preferred by 6 meV/atom. Because the  $2\text{FU-}C2/m$  and  $I4/mmm$  phases are structurally similar, so is their phonon DOS, and their ZPE at 150 GPa is nearly identical. The phonon DOS of the  $5\text{FU-}C2/m$  phase, on the other hand, shows that the frequencies associated with the hydrogen vibrations above  $2000\text{ cm}^{-1}$  are larger in comparison to these two phases, resulting in a significantly larger ZPE at 150 GPa, which leads to the destabilization of this phase when compared to the other two structures. At 200 GPa the ZPE corrections favor the  $I4/mmm$  phase such that its zero-point corrected enthalpy is 25 meV/atom lower than that of  $2\text{FU-}C2/m$ . The reason for this is that the  $C2/m$  structure has more high frequency modes above  $1500\text{ cm}^{-1}$  (see Fig. 5). Thus, our results present another example of how the ZPE of phases with light elements can affect their relative enthalpies. It is beyond the scope of this work to consider anharmonic effects to the (free) energies (and  $T_c$ ), but it may be that these also influence the order of stability of the phases studied herein. To determine if these three  $\text{PH}_2$  structures could potentially contribute to the superconductivity observed by Drozdov and co-workers in their compression of phosphine up to 207 GPa, their superconducting properties were investigated in further detail, as described in the following section.

### Superconducting Phases of $\text{PH}_2$

Above 5 GPa superconductivity has been observed in black phosphorous, the most stable allotrope at ambient conditions. The experimentally measured  $T_c$  depends on the path taken in the pressure/temperature phase diagram. Recent experiments, and DFT calculations using the Allen-Dynes modified McMillan equation, both showed that for the simple cubic phase of phosphorous  $T_c$  decreases with increasing pressure [52, 53]. Computations revealed that the decrease in  $T_c$  above 30 GPa could be explained by the increase in the phonon frequencies, and a  $\mu^*$  of 0.18 yielded a  $T_c$  of 5.8 K at 70 GPa [53], which agrees well with the experimentally measured  $T_c$  of 4.3 K at 100 GPa [52]. At higher pressures, up to 160 GPa, experiments suggested that  $T_c$  decreased below 4 K [52]. In comparison, the computational methodology used herein coupled with a  $\mu^*$  of 0.18 resulted in a  $T_c$  of 6.4 K for simple cubic phosphorous at 100 GPa, and slightly higher temperatures for smaller values of the Coulomb pseudopotential, see Table II. We have also computed the parameters entering the Allen-Dynes modified McMillan equation for simple hexagonal phosphorous at 150 and 200 GPa, so that they may be compared with those calculated for the aforementioned  $\text{PH}_2$  phases. As Table II shows, the average logarithmic frequency,  $\omega_{\log}$ , of phosphorous increases with pressure and the electron-phonon coupling,  $\lambda$ , decreases quenching the superconductivity within the simple hexagonal phase.

How would the incorporation of H atoms within the phosphorus lattices, in the most stable  $\text{PH}_2$  geometries, affect the  $\omega_{\log}$ ,  $\lambda$  and  $T_c$ ? To answer this question we computed the superconducting properties of the previously discussed  $\text{PH}_2$

phases, at pressures where they were found to be dynamically stable, and the results are given in Table II. Fig. 5 provides the phonon band structure and linewidths, Eliashberg spectral function, and plots the dependence of  $\lambda$  on the frequencies for the  $2\text{FU-}C2/m$  and  $I4/mmm$  phases at 200 GPa (analogous plots can be found in the SI for all of the other  $T_c$  values computed herein). In pure compressed hydrogen it has been proposed that  $\mu^*$  can range from 0.08 to 0.089[54, 55], whereas values of 0.18[53] have been employed for simple cubic phosphorus at 100 GPa. We therefore list critical temperatures computed for  $\mu^*$  of 0.1 and 0.18 in Table II. However, because the generally accepted value for the Coulomb pseudopotential is within 0.1 to 0.13, the text quotes  $T_c$  values computed for a  $\mu^*$  of 0.1.

Because of the structural similarities between  $C2/m$  and  $I4/mmm$  at 150 GPa, their critical temperatures should be nearly identical, and  $T_c$  was calculated as being 51 K for the  $I4/mmm$  structure. The aforementioned canting of the octahedra results in geometric changes between these two structures at higher pressures, which could potentially affect the superconducting properties. Indeed, at 200 GPa the electron phonon coupling of  $I4/mmm$  was calculated as being somewhat larger than for  $C2/m$ , but  $\omega_{\log}$  was nearly 175 K larger for  $C2/m$  because the vibrational modes arising primarily from hydrogen atoms are, on average, found at higher frequencies in this phase. The canting results in a larger number of hydrogen atoms that are found within a distance of  $2\text{ \AA}$  of a given hydrogen in  $C2/m$ , thereby increasing the frequencies associated with their vibrations. For example, whereas  $I4/mmm$  has four H-H distances at 1.486  $\text{\AA}$ , in  $C2/m$  the H-H measures are  $1 \times 1.497\text{ \AA}$ ,  $1 \times 1.507\text{ \AA}$ ,  $2 \times 1.585\text{ \AA}$ , and  $2 \times 1.775\text{ \AA}$ . Because of the opposing effects of  $\omega_{\log}$  and  $\lambda$  on the critical temperature, the  $T_c$  values computed for the  $C2/m$  (76 K) and  $I4/mmm$  (70 K) phases at 200 K are very similar despite their structural differences.

At 200 GPa the most significant contribution to  $\lambda$  in the  $2\text{FU-}C2/m$  and  $I4/mmm$   $\text{PH}_2$  systems stems from vibrational modes between  $500\text{-}1750\text{ cm}^{-1}$  that involve hydrogen and phosphorus motions. The electron phonon coupling arising from modes above  $1750\text{ cm}^{-1}$ , which consist primarily of the motion of hydrogen atoms with a small share from the phosphorous atoms, are also substantial components of the total  $\lambda$ . Vibrations below  $500\text{ cm}^{-1}$ , which are the result of phosphorus motions, play a small, but non-negligible role in the electron-phonon coupling. The computed  $T_c$  of the  $\text{PH}_2$  phases are significantly larger than for monoatomic phosphorus because hydrogen increases both  $\omega_{\log}$  and  $\lambda$ . The electron phonon coupling is in-line with the values typically computed for compressed hydrogen-rich phases, 0.5-1.6[56-58], but smaller than the values of 2.19 at 200 GPa and 2.69 at 150 GPa computed for  $I\bar{m}\bar{3}m$   $\text{H}_3\text{S}$  [11] and  $\text{CaH}_6$  [59], respectively. The phonon linewidths reveal that unlike  $\text{CaH}_6$  [59], where the electron phonon coupling was derived primarily from a single vibrational mode, a plethora of modes contribute towards  $\lambda$  in  $\text{PH}_2$ .

The superconducting critical temperatures we compute for

TABLE II: Electron-phonon coupling parameter ( $\lambda$ ), logarithmic average of phonon frequencies ( $\omega_{\log}$ ) and estimated superconducting critical temperature ( $T_c$ ) for values of the Coulomb pseudopotential ( $\mu^*$ ) of 0.1 and 0.18 for simple cubic (S.C.) phosphorous, simple hexagonal (S.H.) phosphorous, and the  $5FU-C2/m$ ,  $2FU-C2/m$ , and  $I4/mmm$   $PH_2$  phases at various pressures.

System	Pressure (GPa)	$\lambda$	$\omega_{\log}$ (K)	$T_c^{\mu^*=0.1}$ (K)	$T_c^{\mu^*=0.18}$ (K)
S.C. P	100	0.66	521.7	15.9	6.4
S.H. P	150	0.21	575.6	0.00	0.00
S.H. P	200	0.13	671.8	0.00	0.00
$5FU-C2/m$	100	1.05	655.1	49.0	32.1
$5FU-C2/m$	150	1.00	798.1	55.5	35.2
$2FU-C2/m$	200	1.04	1026.5	75.6	49.2
$I4/mmm$	150	0.86	946.2	50.6	28.3
$I4/mmm$	200	1.13	851.6	70.4	48.0

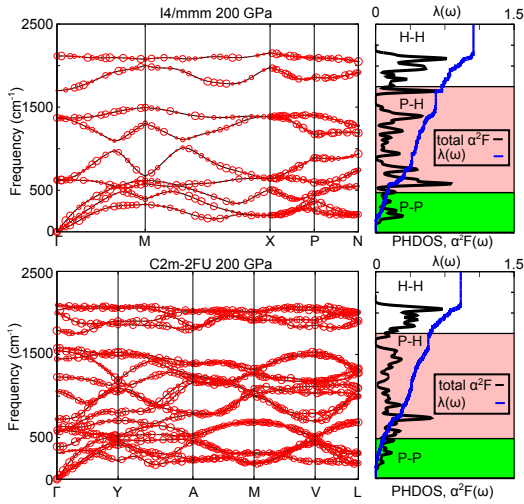


FIG. 5: Phonon band structure, Eliashberg spectral function,  $\alpha^2F(\omega)$ , and the electron-phonon integral,  $\lambda(\omega)$ , for  $2FU-C2/m$  and  $I4/mmm$   $PH_2$  at 200 GPa. Circles indicate the phonon linewidth with a radius proportional to the strength. The highlighted sections of the  $\alpha^2F(\omega)$  plots show the division into vibrational modes that are comprised of phosphorus vibrations (P-P, green), motions of hydrogen and phosphorus atoms (P-H, pink), and mainly hydrogen vibrations (H-H, white). The contribution towards  $\lambda$  for these divisions are 0.09 (9.3%), 0.50 (54.6%), and 0.33 (36.1%) for  $2FU-C2/m$  and 0.13 (12.8%), 0.58 (54.9%), and 0.34 (32.3%) for  $I4/mmm$ , for the green, pink, and white divisions, respectively.

the  $I4/mmm$  and  $2FU-C2/m$  phases of  $PH_2$  are somewhat lower than the experimentally measured value of 103 K at 207 GPa [21]. However, it may be that the  $T_c$  measured by Drozdov and co-workers results from a mixture of phases. For example, recent experimental work has suggested that the decomposition of LiH under pressure in a diamond anvil cell may lead to the formation of layers with different  $LiH_n$  stoichiometries[60]. The experiments were inspired by theoretical predictions[61], and observables computed via DFT calculations were employed to aid the interpretation of the experimental results. Pepin and co-workers suggested that under pressure Li diffuses into the diamond anvil cell forming a

$LiH_6$  layer at the diamond/sample interface, and an  $LiH_2$  layer at the  $LiH_6/LiH$  interface. Such mechanisms may also be important for the pressure induced decomposition of phosphine, and it is only via comparison of the computed experimental observables for specific phases with the results obtained experimentally that one can uncover which phases are formed under pressure, and the mechanisms underlying their formation. A feedback loop between experiment and theory is integral to advance our understanding of high pressure phenomena.

The decrease in  $T_c$  with pressure of all of the  $PH_2$  phases considered herein correlates with the markedly lower critical temperature, 30 K, measured by Drozdov and co-workers at 83 GPa. In future work we will focus on predicting the structures of  $PH_n$  phases at pressures where vdW interactions may be important, and interrogate their bonding and superconducting properties.

## CONCLUSIONS

Recent experiments revealed that when  $PH_3$  is compressed to 207 GPa, it becomes superconducting below 103 K [21]. Our density functional theory (DFT) calculations have shown that at pressures of 100, 150 and 200 GPa  $PH_3$  is thermodynamically unstable with respect to decomposition into the elemental phases, as well as  $PH_2$  and  $H_2$ . Based upon the computed enthalpies other reactions that may occur under pressure are:  $PH_3+H_2 \rightarrow PH_5$  (100 and 150 GPa) and  $PH_2 \rightarrow \frac{1}{2}H_2+PH$  (100 GPa). *A priori* crystal structure prediction has been used to identify three  $PH_2$  phases that are dynamically stable in the pressure range of 100-200 GPa. All of these are calculated to be superconducting via the Allen-Dynes modified McMillan equation, suggesting that like  $H_3S$  [9],  $PH_2$  may be another hydrogen-rich Bardeen-Cooper-Schrieffer (BCS)-type superconductor.

Two  $PH_2$  structures with  $C2/m$  and  $I4/mmm$  symmetry were computed to have a superconducting critical temperature,  $T_c$ , of 76 K and 70 K, respectively, at 200 GPa. Between 150-200 GPa the non-ZPE (zero point energy) corrected enthalpies of these phases differed by only a few meV/atom,

and their structures both consisted of square nets of phosphorous atoms. In the  $I4/mmm$  structure the phosphorous atoms were octahedrally coordinated, with two hydrogen atoms in the axial positions. In the  $C2/m$  phase the hydrogens are slightly canted from the ideal octahedral angles allowing the distance between the planes of phosphorous atoms to decrease, and reducing the volume of the structure. A five formula unit phase with  $C2/m$  symmetry (5FU- $C2/m$ ), which consists of 1-D  $\text{PH}_3\text{-PH-PH}_2\text{-PH-PH}_3$  oligomers, was also identified in our evolutionary searches, and it has the lowest non-ZPE corrected enthalpy at 100 GPa. At this pressure its  $T_c$  is computed to be 49 K. Upon decreasing the pressure, the  $T_c$  of all of the  $\text{PH}_2$  phases decreased.

Our results provide another example of how pressure can lead to the formation of compounds with stoichiometries and properties that would not be predicted based upon our experience at 1 atm. Comparison of the observables computed for these  $\text{PH}_2$  phases with results obtained experimentally will unveil which phase, or mixture of phases, give rise to the superconducting properties observed by Drozdov and co-workers [21].

*Supplementary Information Available:* Details of the structure searches, band structures, structural parameters, DOS plots, phonon DOS plots, absolute energies in Hartree, phonon convergence plots, and Nudged Elastic Band results. This material is available free of charge via the Internet at <http://pubs.acs.org>.

## ACKNOWLEDGEMENTS

We acknowledge the NSF (DMR-1505817) for financial, and the Center for Computational Research (CCR) at SUNY Buffalo for computational support. A.S. acknowledges financial support from the Department of Energy National Nuclear Security Administration under Award Number DE-NA0002006, and E.Z. thanks the Alfred P. Sloan Foundation for a research fellowship (2013-2015). A.S. also acknowledges Daniel Miller for his help with using the Nudge Elastic Band Method.

---

\* Electronic address: [ezurek@buffalo.edu](mailto:ezurek@buffalo.edu)

- [1] W. Grochala, R. Hoffmann, J. Feng and N. W. Ashcroft, *Angew. Chem. Int. Ed.*, **2007**, *46*, 3620–3642.
- [2] E. Zurek and W. Grochala, *Phys. Chem. Chem. Phys.*, **2015**, *17*, 2917–2934.
- [3] Hermann, A.; Schwerdtfeger, P. *J. Phys. Chem. Lett.* **2014**, *5*, 4336–4342.
- [4] Hermann, A.; McSorley, A.; Ashcroft, N. W.; Hoffmann, R. *J. Am. Chem. Soc.* **2012**, *134*, 18606–18618.
- [5] Peng, F.; Miao, M.; Wang, H.; Li, Q.; Ma, Y. *J. Am. Chem. Soc.* **2012**, *134*, 18599–18605.
- [6] Peng, F.; Yao, Y.; Liu, H.; Ma, Y. *J. Phys. Chem. Lett.* **2015**, *6*, 2363–2366.
- [7] Lu, C.; Miao, M.; Ma, Y. *J. Am. Chem. Soc.* **2013**, *135*, 14167–14171.
- [8] Yao, Y.; Hoffmann, R. *J. Am. Chem. Soc.* **2011**, *133*, 21002–21009.
- [9] Drozdov A. P., Eremets M. I., Troyan I. A., Ksenofontov V. and Shylin S. I., *Nature*, **2015**, *525*, 73–76.
- [10] Y. Li, J. Hao, H. Liu, Y. Li and Y. Ma, *J. Chem. Phys.*, **2014**, *140*, 174712.
- [11] D. Duan, Y. Liu, F. Tian, D. Li, X. Huang, Z. Zhao, H. Yu, B. Liu, W. Tian and T. Cui, *Sci. Rep.*, **2014**, *4*, 6968.
- [12] J. A. Flores-Livas, A. Sanna and E. K. U. Gross, arXiv:1501.06336v1.
- [13] D. A. Papaconstantopoulos, B. M. Klein, M. J. Mehl and W. E. Pickett, *Phys. Rev. B*, **2015**, *91*, 184511.
- [14] N. Bernstein, C. S. Hellberg, M. D. Johannes, I. I. Mazin and M. J. Mehl, *Phys. Rev. B*, **2015**, *91*, 060511.
- [15] D. Duan, X. Huang, F. Tian, D. Li, H. Yu, Y. Liu, Y. Ma, B. Liu and T. Cui, *Phys. Rev. B*, **2015**, *91*, 180502.
- [16] I. Errea, M. Calandra, C. J. Pickard, J. Nelson, R. J. Needs, Y. Li, H. Liu, Y. Zhang, Y. Ma and F. Mauri, *Phys. Rev. Lett.*, **2015**, *114*, 157004.
- [17] R. Akashi, M. Kawamura, S. Tsuneyuki, Y. Nomura and R. Arita, *Phys. Rev. B*, **2015**, *91*, 224513.
- [18] X. Zhong, H. Wang, J. Zhang, H. Liu, S. Zhang, H. Song, G. Yang, L. Zhang and Y. Ma, arXiv:1502.02607.
- [19] Y. Li, L. Wang, H. Liu, Y. Zhang, J. Hao, C. J. Pickard, J. R. Nelson, R. J. Needs, W. Li, Y. Huang, I. Errea, M. Calandra, F. Mauri and Y. Ma, arXiv:1508.03900.
- [20] N. W. Ashcroft, *Phys. Rev. Lett.*, **2004**, *92*, 187002.
- [21] A. P. Drozdov, M. I. Eremets and I. A. Troyan, arXiv:1508.06224.
- [22] Y. Fu, X. Du, L. Zhang, F. Peng, M. Zhang, C. Pickard, R. J. Needs, D. J. Singh, W. Zheng, Y. Ma, arXiv:1510.04415.
- [23] D. C. Lonie and E. Zurek, *Comput. Phys. Commun.*, **2011**, *182*, 372–387.
- [24] D. C. Lonie and E. Zurek, *Comput. Phys. Commun.*, **2011**, *182*, 2305–2306.
- [25] P. Baettig and E. Zurek, *Phys. Rev. Lett.*, **2011**, *106*, 237002.
- [26] J. Hooper and E. Zurek, *Chem. Eur. J.*, **2012**, *18*, 5013–5021.
- [27] J. Hooper and E. Zurek, *ChemPlusChem*, **2012**, *77*, 969–972.
- [28] A. Shamp, J. Hooper and E. Zurek, *Inorg. Chem.*, **2012**, *51*, 9333–9342.
- [29] J. Hooper, T. Terpstra, A. Shamp and E. Zurek, *J. Phys. Chem. C*, **2014**, *118*, 6433–6447.
- [30] D. C. Lonie and E. Zurek, *Comput. Phys. Commun.*, **2012**, *183*, 690.
- [31] G. Kresse and J. Hafner, *Phys. Rev. B*, **1993**, *47*, 558.
- [32] J. P. Perdew, K. Burke and M. Ernzerhof, *Phys. Rev. Lett.*, **1996**, *77*, 3865.
- [33] P. Blöchl, *Phys. Rev. B*, **1994**, *50*, 17953.
- [34] S. Gohr, S. Grimme, T. Soehnel, B. Paulus and P. Schwerdtfeger, *J. Chem. Phys.*, **2013**, *139*, 174501.
- [35] D. Sheppard, P. Xiao, W. Chemelewski, D. D. Johnson, and G. Henkelman, *J. Chem. Phys.*, **2012**, *136*, 074103.
- [36] P. Giannozzi, S. Baroni, N. Bonini, M. Calandra, R. Car, C. Cavazzoni, D. Ceresoli, G. L. Chiarotti, M. Cococcioni, I. Dabo, A. Dal Corso, S. de Gironcoli, S. Fabris, G. Fratesi, R. Gebauer, U. Gerstmann, C. Gougoussis, A. Kokalj, M. Lazzeri, L. Martin-Samos, N. Marzari, F. Mauri, R. Mazzarello, S. Paolini, A. Pasquarello, L. Paulatto, C. Sbraccia, S. Scandolo, G. Sclauzero, A. P. Seitsonen, A. Smogunov, P. Umari and R. M. Wentzcovitch, *J. Phys. Condens. Matter*, **2009**, *21*, 395502.
- [37] P. B. Allen and R. C. Dynes, *Phys. Rev. B*, **1975**, *12*, 905.



- [38] C. J. Pickard and R. J. Needs, *Nat. Phys.*, **2007**, *3*, 473–476.
- [39] C. J. Pickard, M. Martinez-Canales and R. J. Needs, *Phys. Rev. B*, **2012**, *85*, 214114.
- [40] T. Kikegawa and H. Iwasaki, *Acta Cryst.*, **1983**, *B39*, 158–164.
- [41] S. M. Clark and J. M. Zaug, *Phys. Rev. B.*, **2010**, *82*, 134111.
- [42] Y. Akahama, M. Kobayashi and H. Kawamura, *Phys. Rev. B.*, **1999**, *59*, 8520.
- [43] Y. Akahama, H. Kawamura, S. Carlson, T. L. Bihan and D. Hausermann, *Phys. Rev. B*, **2000**, *61*, 3139.
- [44] J. C. Jamieson, *Science*, **1963**, *139*, 1291–1292.
- [45] D.-K. Seo and R. Hoffmann, *J. Solid State Chem.*, **1999**, *147*, 26–37.
- [46] S. E. Boulfelfel, G. Seifert, Y. Grin and S. Leoni, *Phys. Rev. B.*, **2012**, *85*, 014110.
- [47] F. J. H. Ehlers and N. E. Christensen, *Phys. Rev. B*, **2004**, *69*, 214112.
- [48] U. Hausserman, *Chem. Eur. J.*, **2003**, *9*, 1471–1478.
- [49] G. W. C. Kaye and T. H. Laby, *Tables of Physical and Chemical Constants*, 1995, <http://www.kayelaby.npl.co.uk/>.
- [50] R. C. Weast and S. M. Selby, *Handbook of Chemistry and Physics*, **1966**, CRC Press/Taylor and Francis, Boca Raton, FL.
- [51] J. Hooper, B. Altintas, A. Shamp and E. Zurek, *J. Phys. Chem. C*, **2012**, *117*, 2982-2992.
- [52] M. Karuzawa, M. Ishizuka and S. Endo, *J. Phys. Condens. Matter*, **2002**, *14*, 10759–10762.
- [53] K. T. Chan, B. D. Malone and M. L. Cohen, *Phys. Rev. B*, **2013**, *88*, 064517.
- [54] C. F. Richardson and N. W. Ashcroft, *Phys. Rev. Lett.*, **1997**, *78*, 118.
- [55] J. M. McMahon and D. M. Cohen, *Phys. Rev. B*, **2011**, *84*, 144515.
- [56] J. A. Flores-Livas, M. Amsler, T. J. Lenosky, L. Lehtovaara, S. Botti, M. A. L. Marques and S. Goedecker, *Phys. Rev. Lett.*, **2012**, *108*, 117004.
- [57] G. Gao, A. R. Oganov, A. Bergara, M. Martinez-Canales, T. Cui, T. Iitaka, Y. Ma and G. Zou, *Phys. Rev. Lett.*, **2008**, *101*, 107002.
- [58] J. S. Tse, T. Yao and K. Tanaka, *Phys. Rev. Lett.*, **2007**, *98*, 117004.
- [59] H. Wang, J. S. Tse, K. Tanaka, T. Iitaka and Y. Ma, *Proc. Natl. Acad. Sci. USA*, **2012**, *109*, 6463–6466.
- [60] C. Pepin, P. Loubeyre, F. Occelli, and P. Dumas, *Proc. Natl. Acad. Sci. USA*, **2015**, *112*, 7673-7676.
- [61] E. Zurek, R. Hoffmann, N. W. Ashcroft, A. R. Oganov, and A. O. Lyakhov, *Proc. Natl. Acad. Sci. USA*, **2009**, *106*, 17640-17643.